POLITECNICO DI TORINO
Repository ISTITUZIONALE

Reliability-based design of rockfall passive systems height

Terms of use:

(Article begins on next page)

11 April 2024

Reliability-based design of rockfall passive systems height[☆]

Maddalena Marchelli[a,*], Valerio De Biagi[b], Daniele Peila[a]

[a]*DIATI, Department of Environment, Land and Infrastructure Engineering, Politecnico di Torino, Corso Duca degli Abruzzi 24, 10129 Torino, Italy*
[b]*DISEG, Department of Structural, Geotechnical and Building Engineering, Politecnico di Torino, Corso Duca degli Abruzzi 24, 10129 Torino, Italy*

Abstract

Passive structural systems against rockfalls, as net fences and embankments, are among the most effective mitigation measures for high energy events. Although largely adopted, the design of these systems has not been codified yet. A profitable time-dependent reliability approach has been recently introduced by the Authors, accounting for different possible probability distributions of velocity, mass, and height of the impacting block. Two failure modes were considered, related to the energy absorption capacity and the intercepting height of the systems. As the current design approach is based on partial safety factors, several sensitivity analyses are herein presented, with a particular focus on the height, firstly to define a suitable combination of equivalent partial safety factors, and, secondly, to investigate the parameters related to the geometry and the kinematics of the block which mostly affect the factors. Moreover, for a given failure probability, two shallow neural network were built, one for each failure mode, considering the possible range of all the input parameters, creating thus two input-output relationships that can be used to evaluate the partial safety factors for the height and the energy.

Keywords: rockfall, reliability analysis, partial safety factors, net fence,

1. Introduction

Among the natural hazards, rockfalls constitute a serious threat to life, properties and infrastructures, due to their spatial and temporal unpredictability and high energy involved [1, 2]. This kind of event can severely affect civil structures and infrastructures as hamlets, roads, railways [3, 4, 5] but has also industrial implications related, e.g. to quarries and open pit mines, also linked with the optimization of the orebody exploitation process [6, 7, 8, 9]. As a consequence, rockfall risk reduction can represent one of the most significant aspects in various engineering and human activities. Concern about passive mitigation measures has become a central issue in rockfall risk management [10, 11] and, as a result, much research in the last decades has focused on the development of new technologies. Among these structures, rockfall net fences and embankments represent the most effective solutions in case of events characterized by large energy and/or high trajectories [12]. The design of these protection measures is still under debate and a standardized procedure is not yet available, due both to the complexity of the problem and to the several technologies adopted [13, 14, 15, 16, 17]. Nowadays, following the CE marking procedure [18], the design of the net fences is oriented towards a performance-based design approach, evaluating energy absorption capacity and height. On the contrary, no codified procedure exists either for CE making and the design of rockfall embankments [19, 20].

The understanding and the modelling of the rockfall phenomenon is difficult to achieve [21] as appropriate assumptions, e.g. considering the source zone location [22], the initial released volume and the impacting volume [23] have to be made. Simplifications concerning the direction of the impact on the barrier or the precise position of the system along the slope are generally introduced. Few papers analyze these aspects [24, 25, 26, 27] and the different resisting mechanisms that can arise in passive protection system according to the impacting block volume [28, 29] and the impacted element [30]. Although complex numerical models have been realized [31, 32, 33], the coupling between the impacting block and a retaining structure is tricky, and difficulties often arise when merging the results of trajectory analyses and the model of a net fence or an embankment [34].

Mimicking the performance-based design approach, i.e. starting from the assumption that the failure of the system can occur for block kinetic energies or trajectory heights greater than the interception capacity of the system, and the current practice based on the Eurocode 0 [35], the present work aims at identifying a compelling solution for the design of these retaining systems. This procedure is based on a time-dependent reliability-based approach introduced in De Biagi et al. [36], discussed in Marchelli et al. [37], and here enhanced (Sec. 2), which considers all the possible distributions of the velocity, mass and height of the block impacting against the protective system located in an arbitrary position along the slope. With the aim of merging it with the ultimate limit state procedure suggested in the Eurocodes [35, 38], which is based on safety factors applied to resistance and actions, equivalent partial safety factors for the impacting block energy and height were derived, with particular focus on the intercepting height of the systems.

Different combinations were analyzed, considering or not a mutual independence between the two failure modes (Sec. 3.1). Sensitivity analyses were performed to investigate the parameters which mostly affect the adopted partial safety factors (Sec. 4). As already illustrated in the papers by the Authors previously cited, the values of the factors largely depend upon many variables. With the aim of providing a profitable tool for the design of such structures, a shallow neural network was built in order to create two input-output relationships that can be used to evaluate the partial safety factors for the height and the energy, given a failure probability (Sec. 5). At the end, conclusions and future perspective were suggested (Sec. 6).

2. Time-dependent reliability approach

This section provides the fundamental principles of the reliability approach adopted for rockfall protection structures. The proposed method constitutes an improvement of the method proposed in [36] and discussed in [37]. Basically, rockfall passive mitigation measures as net fences and embankments have to intercept a falling block and withstand its dynamic impact without exceedingly deforming, breaking, or collapsing. As a result, the possible failure modes of these structures can be simplified into a failure mode related to the exceeding height (to which a failure probability F_h is associated) when the block is not intercepted, and one related to the exceeding kinetic energy, F_k, when the absorption capacity of the system, i.e. reference energy capacity evaluated according to the assessment procedure

3

of EAD 340059-00-0106 [18], is smaller than block translational energy. The total failure probability of the system p_f accounts for both modes and can be precautionary considered as the sum of the failure probabilities F_h and F_k [36]. Each of the two failure modes represents a scenario mathematically described through a limit function, i.e. the boundary between failure and safety, derived from a state function. The limit function allows to assess the reliability of a system or, vice versa, for a given failure probability p_f, to obtain the design values of the variables (denoted with subscript $_d$) composing the state function. Considering the temporal variability of some of the variables, e.g. the mass of the impacting block, the proposed approach is time-integrated. For a given return period T, the mass is assumed to follow a normal distribution, whose mean value $m_{50}(T)$ can be computed through a power-law rule, as suggested in [39]:

$$m_{50}\left(T\right) = M_{th}\left(\lambda T\right)^{1/\alpha},\tag{1}$$

where α is the shape coefficient of a Pareto Type I distribution accounting for the heterogeneity of the size of the possible impacting blocks, M_{th} is the threshold mass, i.e. the minimum mass of an impacting block whose occurrence frequency is λ. Refer to [39] for details about the law. The ratio between the standard deviation and the mean value, named $COVm$ represents the spread of the distribution. The estimation of the heterogeneity of the blocks in the location where the passive structural system is assumed to be installed is obviously function of the number of observed blocks N that lead to the estimation of the shape coefficient α.

In the following, the failures modes are presented. In the analysis, lumped-mass assumptions were considered, i.e neglecting the influence of block mass on its kinematics. The restitution coefficients were normally distributed whose mean values are selected to account for the variability of block-slope interaction phenomena.

2.1. Failure due to the exceeding height

The analysis of the failure mode associated to exceeding trajectory height accounts for the variability of the impacting block size (or mass), which can differ from event to event. F_h represents the probability associated to this failure mode and encompasses all the possible rock block sizes that can fall along the slope. Considering that an event occurs, the probability of failure due to exceeding height, $p_{fa,h}$, depends on the occurrence of specific

probability distributions of the mass, m, and of the height of the impacting block, h_b, described through quantities defined as representative, namely the characteristic values (denoted with subscript $_k$):

$$p_{fa,h} = \int_0^\infty \int_0^\infty p_{fh}| \left(m_k = \mu \text{ and } h_{b,k} = \eta \right) f_{m_k,h_{b,k}} \left(\mu, \eta \right) d\mu \ d\eta, \quad (2)$$

where $f_{m_k,h_{b,k}} \left(\mu, \eta \right)$ is the joint probability density function of having a distribution of masses and heights defined through their characteristic values that assumes the values of μ and η, respectively, considered as random variables. Under the lumped-mass assumption, it can be assumed that the trajectory height of the block does not depend on the mass [40, 41, 42, 43] and, consequently, $f_{m_k,h_{b,k}} \left(\mu, \eta \right)$ is equal to the product of the single probability density functions, i.e. f_{m_k} and $f_{h_{b,k}}$. Relaxing the assumptions, the simplification cannot be performed and, thus, the joint probability density function depends both on the mass and on trajectory height. Thus, the integral of Eqn. (2) should be numerically performed. Provided that the block releasing conditions remain unchanged in terms of location and initial velocity, for a given slope, the lumped-mass trajectory analysis outputs a unique distribution of the heights, independently from the released volume, resulting in $f_{h_{b,k}}$ equal to one. Hence, Eqn. (2) turns into:

$$p_{fa,h} = \int_0^\infty p_{fh}| \left(m_k = \mu \right) f_{m_k} \left(\mu \right) d\mu. \quad (3)$$

The probability density function $f_{m_k} \left(\mu \right)$ related to the distribution of the mass, referred through its characteristic value m_k, differing for each T (Eqn. (1)), can be described through a Pareto Type I distribution, according to [44], as:

$$f_{m_k} \left(\mu \right) = \begin{cases} 0 & \mu < M_{th} \\ \frac{\alpha}{M_{th}} \left(\frac{\mu}{M_{th}} \right)^{-\alpha-1} & \mu \geq M_{th} \end{cases}. \quad (4)$$

The conditional failure probability $p_{fh}| \left(m_k = \mu \right)$ is studied through a state function accounting for the exceeding of the protection system height, h_B, expressed as:

$$H \left(\mathbf{h} \right) = H \begin{pmatrix} h_B \\ h_b \\ m \end{pmatrix} = h_B - h_b - \sqrt[3]{\frac{3m}{4\pi\rho}}, \quad (5)$$

where ρ is the density of the block. This formulation considers that h_b is evaluated in the center of mass of the impacting block and, consequently, a tolerance of half of its characteristic dimension has to be inserted. In the present work, a spherical block is assumed. Finally, the conditional failure probability $p_{fh}|\,(m_k = \mu)$ related to the state function is computed as:

$$p_{fh}|\,(m_k = \mu) = P\,(H\,(\mathbf{h})\,|\,(m_k = \mu) \leq 0) = \iiint\limits_{H(\mathbf{h}) \leq 0} f_H|\,(m_k = \mu)\,(\mathbf{h})\ dh_B\ dh_b\ dm,$$

$$(6)$$

where $f_H|\,(m_k = \mu)$ is the joint probability density function of the mass (with characteristic value equal $m_k = \mu$) and the height of the impacting block, and the nominal height of the protection system. Following the approach reported in [36], the failure probability in a given time period, τ, which can be assumed equal to one year or to the expected working life of the protection system, can be obtained as:

$$\mathrm{F}_h\,(\tau) = p_{f,h}\,(t) \approx 1 - \exp\,(-\nu\tau p_{fa,h}),\tag{7}$$

where ν can be assumed equal to λ.

2.2. Failure due to the exceeding kinetic energy

The study related to failure mode associated to exceeding kinetic energy was recently reported by the Authors in previous papers [36, 37]. Briefly, the state function accounting for the exceeding of the system energy capacity, E_B, expressed as:

$$K\,(\mathbf{e}) = K\begin{pmatrix} E_B \\ m \\ v \end{pmatrix} = E_B - \frac{1}{2}mv^2,\tag{8}$$

where v is the impacting block velocity. The proposed equation lacks for the rotational term as it has been demonstrated that the influence of this last on the global failure of the system is negligible [45, 46]. This assumption is consistent with the full scale tests conducted to assess the performance of a rockfall flexible barrier [18]. Under the lumped-mass assumption, as for the failure mode associated to exceeding height, the trajectory analysis provides a unique distribution of the velocity and, thus a unique characteristic value of the velocity can be defined. Relaxing the lumped-mass assumptions, considerations similar to the ones proposed for the other failure mode can be

6

proposed. As a result, the conditional failure probability $p_{fe}|\left(m_k = \mu\right)$ can be computed as:

$$p_{fe}|\left(m_k = \mu\right) = P\left(K\left(\mathbf{e}\right)|\left(m_k = \mu\right) \leq 0\right) = \iiint\limits_{K(\mathbf{e}) \leq 0} f_E|\left(m_k = \mu\right)\left(\mathbf{e}\right) \; dE_B \, dm \, dv,$$

(9)

where $f_E|\left(m_k = \mu\right)$ is the joint probability density function of the mass (with characteristic value equal $m_k = \mu$) and the velocity of the impacting block, and the barrier capacity. The failure probability due to exceeding kinetic energy in a given time period τ is computed as:

$$\mathrm{F}_k\left(\tau\right) = p_{f,k}\left(t\right) \approx 1 - \exp\left(-\nu \tau p_{fa,k}\right).$$

(10)

3. Equivalent partial safety coefficient: different combinations

The reliability level of a structure is related to a specific failure probability. The proposed approach can be alternatively considered for the design or for the calibration of the partial safety factors to be adopted in the current semi-probabilistic design framework [47]. The partial safety factors, namely γ in the design codes, say [35], are coefficients (always larger than one) that serve for computing the design value of the variable, usually denoted with subscript $_d$, from its characteristic value. The design value of the action is the product between the characteristic value and the factor, while the design value of the resistances is the ratio between the characteristic value and the factor. In this specific problem, different partial safety factors related to the actions, i.e. the impacting block parameters, can be individuated: considering its mass, height, and velocity as representative, three partial safety factors, namely, γ_m, γ_h and γ_v, can be defined. The semi-probabilistic approach generally applies a partial safety factor also to each resistance parameter, i.e. in the specific case, to the nominal height h_B (named γ_{h_B}) and to the energy absorption capacity E_B of the system (named γ_{E_B}). Merging with the current practice, the calculations can be simplified by considering the values of the absorption capacity E_B and the CE certified nominal height h_B as Dirac-δ distributions, and, thus, the design value is assumed equal to the characteristic one. All these coefficients can be merged in a unique factor for each failure mode, i.e. γ_H and γ_E, for the failure mode associated to the height and the energy, respectively.

Referring to the European standards, the Italian recommendation UNI 11211-4 [48] applies a partial safety factor for each variable, assuming as

characteristic values of the actions the 95th percentiles of the trajectory height and velocity distributions of the block, i.e. $h_k = h_{95}$ and $v_k = v_{95}$, while for the impacting block mass the choice of the characteristic value is remitted to the designer with the condition that it has to be assumed equal or greater than the 95th percentile of the distribution of possible masses. On the contrary, in the Austrian recommendation [49], the characteristic mass is defined as a given percentile depending by the occurrence probability of a rockfall event and the consequence class of the elements at risk. Furthermore, ONR 24810 [49] accounts for a unique partial safety term related to the action for each failure mode, considering a characteristic value of the kinetic energy of the impacting block, assumed equal to the 99th percentile of the energy distribution. The characteristic value of the height is computed as the sum between the 95th percentile of the trajectory height of the characteristic block and half of its maximum dimension. In the end, considering the effects of the resistance, both standards accounts for a partial safety factor for the energy absorption capacity of the system, while only ONR 24810 [49] applies a partial safety factor to the nominal height of the system.

The present research work aims at finding a profitable solution for the designer, merging the proposed reliability-based approach with the current semi-probabilistic one, finding the simplest way for introducing the uncertainties related to the phenomenon (i.e. the kinematics of the block) into the design process. This results in choosing the most suitable combination of partial safety factors to adopt, i.e. one for each variable, or one for the effect of the actions and of the resistance, or a unique for each failure mode. In addition, as the variable related to the mass of the impacting block affects both the two failure modes, the corresponding partial safety factor can be taken as a unique value for each mode.

With particular reference to the exceeding height failure mode (with failure probability F_h), three different combinations of partial safety factors can be identified:

1. different partial safety factors for each variable, assuming a mutual independence between the two failure modes [36]:

$$\frac{h_B}{\gamma_{h_B}} = \gamma_{h_b} h_{b,k} + \left(\frac{3}{4\pi\rho} \gamma_{m_h} \ m_k \right)^{1/3}, \qquad (11)$$

where γ_{h_B} is the factor related to the height of the system, γ_{h_b} to the height of the trajectory, and γ_{m_h} to the size of the block (the mass).

8

The γ_{m_h} differs from the factor of the mass computed to achieve a given failure probability due to exceeding kinetic energy;

2. different partial safety factors for each variable, adopting, for the mass, the same factor γ_{m_E} evaluated computing the failure related to the kinetic energy, F_k:

$$\frac{h_B}{\gamma_{h_B}} = \gamma_{h_b}^* h_{b,k} + \left(\frac{3}{4\pi\rho} \gamma_{m_E} m_k \right)^{1/3}, \tag{12}$$

where

$$\gamma_{h_b}^* = \frac{1}{h_{b,k}} \left[\frac{h_B}{\gamma_{h_B}} - \left(\frac{3}{4\pi\rho} \gamma_{m_E} m_k \right)^{1/3} \right]. \tag{13}$$

Obviously, $\gamma_{h_b} \neq \gamma_{h_b}^*$;

3. a unique safety factor for the effect of the actions:

$$\frac{h_B}{\gamma_{h_B}} = \gamma_{H'} \left[h_{b,k} + \left(\frac{3}{4\pi\rho} m_k \right)^{1/3} \right]. \tag{14}$$

Merging the factors related to the effects of the action and of the resistance, the last combination (Eqn. (14)) can be simply rewritten as:

$$h_B = \gamma_H \left[h_{b,k} + \left(\frac{3}{4\pi\rho} m_k \right)^{1/3} \right], \tag{15}$$

where γ_H includes the effects of both actions ($\gamma_{H'}$) and resistances (γ_{h_B}).

In the calculations that follows, the characteristic and the design protection system heights are assumed equal, and thus, neglecting model uncertainties, γ_{h_B} can be considered equal to 1, and, consequently $\gamma_{H'} = \gamma_H$.

In the present research work, according to the aforementioned national recommentations [48], the 95th percentile of the distribution of the velocity and the height of the block were assumed as characteristic values. Referring to the mass, accounting for its variability in time, a reference time period T_k was considered, and the associated mean value $m_{50}(T_k)$ was adopted as characteristic value. This hypothesis differs from the national recommendations, which do not tackle the temporal problem, even.

3.1. Through the most efficient solution

Aiming at evaluating the most efficient and easy-to-use solution to treat the problem, the three aforementioned combinations of the partial safety factors were examined through a parametric analysis. According to the previous works by the Authors [36, 37], all the variables which can affect the failure of the system were considered, assuming an annual failure probability p_f of 10^{-4} (and thus $\tau = 1$,), equally distributed between F_h and F_k, i.e. $F_h = F_k = 0.5p_f$. The adopted values of the variables for the parametric analysis encompass the most probable real situations, as found in Marchelli et al. [37]. The density of the block is assumed equal to 2700 kg/m³, the reference return period T_k equal to 50, 100, and 200 years and the value of $COVm$ was defined according to the approximate expression [37]:

$$COVm \approx 1.3606 \frac{(\lambda T)^{0.3}}{N^{0.525}\alpha}. \tag{16}$$

The value of the parameter α, as well as the number of surveyed blocks N and the frequency of an event λ are thoroughly site specific, and thus a great variability was assumed precautionary. A number of event spanning from each 2 and 10 years were supposed, with α between 0.8, i.e. heterogeneous deposit, and 1.3, i.e. very homogeneous deposit. The number of surveyed blocks N varies between 300 and 1000. The volume associated to the threshold mass M_{th} (V_{th}) varies from 0.5 m³ to 1.5 m³. As proven in the previous work [36], the adopted characteristic value of the distribution of the impacting block velocity does not affect the result, thus it was assumed equal to 20 m/s, while the ratio v_{99}/v_{95} characterizing the tail of the distribution plays an important role. As reported in De Biagi et al. [36], the right tails of the distribution of height and velocity are approximated with normal distributions. For v_{99}/v_{95}, values spanning from 1.01 and 1.03 were considered. The height of the impacting block was assumed between 2 m and 6 m, while the ratio h_{99}/h_{95} between 1.1 and 1.3. The design values of the variables were computed applying the reliability detailed in Sec. 2, and all the possible combinations of the above-mentioned parameters were evaluated and all the partial safety factors computed according to Eqn. (11), Eqn. (12), and Eqn. (14).

Figure 1 displays the boxplots of the partial safety factors for the three combinations in the case $T_k = 100$ years, revealing their variation.Through this representation, the degree of dispersion, the skewness, and the presence

of outliers values can be appreciated and discussed. The median value is indicated by the central red line, while the bottom and the top edges indicate the 25th (Q_1) and 75th (Q_3) percentiles, respectively. The top of the upper whisker is located at $Q_3 + 1.5\,(Q_3 - Q_1)$. Larger values, namely, the outliers, are plotted as red crosses. Different trends can be observed among all the partial safety factors. Considering the first combination, γ_h displays a left-skewed boxplot (i.e. a negative skew), with a wide upper quartile and several values over the upper whisker limit. Neglecting these lasts, the value of γ_{h_b} spans between 1.20 and 2.24. The boxplot of γ_{m_h} shows several values over the upper whisker limit, set at 1.20, and a narrow interquartile range. Referring to the second combination, an opposite tendency can be observed: a narrow interquartile range for $\gamma_{h_b}^*$, with values spanning between 1 and 1.92, accounting for the whisker; while γ_{m_h}, related to the failure due to exceeding kinetic energy, shows very high values with an upper whisker limit set at 5.38, and two outliers at about 7.1. The third combination, accounting for a unique partial safety factor, displays a slightly left-skewed boxplot, without values over the last quartile, meaning that the minimum and the maximum values coincide with the whisker limits, at about 1.16 and 1.69, respectively.

Table 1 reports the relevant values, i.e. minimum and maximum and whisker limits, accounting for the different reference return periods T_k. The minimum value coincides in all the cases with the lower whisker limit. Concerning the first combination, the influence of T_k is more evident for γ_{h_b} than for γ_{m_h}, but several outliers are observed for γ_{m_h}, increasing the uncertainties related to its value. The second combination highlights very high values of γ_{m_e}, which tends to be greater as T_k decreases. Conversely, γ_H exhibits maximum values coincident with the upper whisker limits, for all the T_k investigated. The observed values span between a minimum of 1.10 for T_k equal to 200 years and a maximum of 2.01 for T_k equal to 50 years.

The performed analyses lead to identify the third combination, expressed through Eqn. (14), as the most affordable and straightforward solution since it is characterized by a smaller dispersion of a single partial safety factor. In addition, in this case, a partial safety factor accounting for the effects of the resistance can be easily introduced. This would be mathematically possible by turning the barrier height into a random variable described by a distribution (say normal) and repeating the reliability analysis previously described.

Starting from this assumption, the present research work analyses the
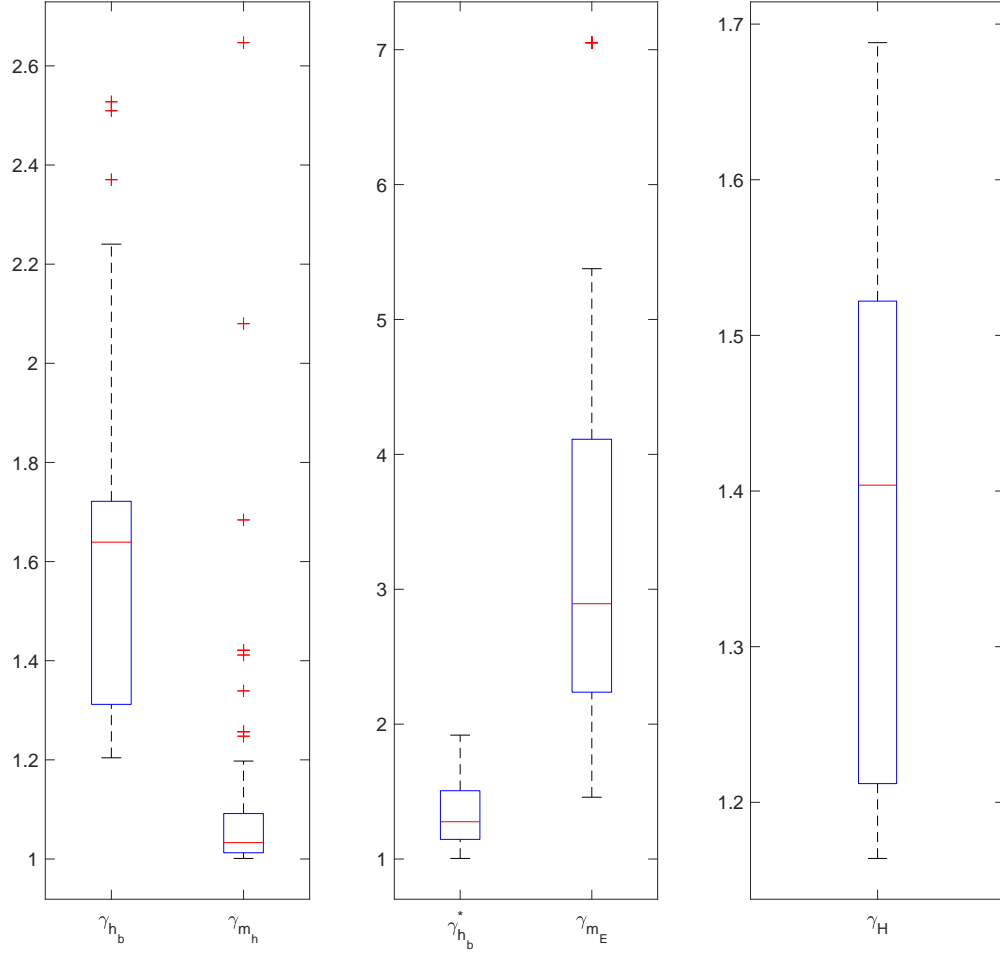
Figure 1: Boxplot of the partial safety factors γ_{h_b}, γ_{m_h}, $\gamma_{h_b}^*$, γ_{m_E}, and γ_H for $T_k = 100$ years.

		T_k **(years)**		
		50	100	200
γ_{h_b}	minimum	1.2334	1.2042	1.1464
	upper whisker limit	2.4103	2.2402	1.8388
	maximum (outliers included)	3.0913	2.5276	1.8388
γ_{m_h}	minimum	1.0006	1.0001	1.0020
	upper whisker limit	1.1256	1.1975	1.2946
	maximum (outliers included)	2.3163	2.6469	2.5609
$\gamma_{h_b}^*$	minimum	1.0961	1.0043	0.7314
	upper whisker limit	2.1498	1.9185	1.7200
	maximum (outliers included)	2.4204	1.9185	1.7200
γ_{m_E}	minimum	1.5828	1.4581	1.3085
	upper whisker limit	7.4741	5.3765	3.9802
	maximum (outliers included)	10.2252	7.0523	3.9802
γ_H	minimum	1.2032	1.1639	1.1012
	upper whisker limit	2.0136	1.6881	1.5999
	maximum (outliers included)	2.0136	1.6881	1.5999

Table 1: Values of of the partial safety factors γ_{h_b}, γ_{m_h}, $\gamma_{h_b}^*$, γ_{m_E} and γ_H for different reference return periods T_k.

influence of the different input variables in the evaluation of γ_H.

4. Influence of the variables on γ_H

The purpose of this section is to deeply investigate the influence of the input variables on the value of the partial safety factor γ_H. The adopted variables are within a range that encompasses the majority of the scenarios that can occur in a real slope [37]. Although an annual failure probability p_f equal to 10^{-4} is considered for the study, it has to be remembered that p_f has to be properly chosen according to a risk analysis. Following Authors' judgment, the chosen p_f is realistic and can be applied in the majority of real cases on engineered slopes. As already illustrated, although the design parameters are fixed for a specific site, the value of the coefficient depends on the chosen return period T_k of the characteristic mass. It is worth recalling that in the proposed time-dependent reliability method, for a given site, the integration of Eqn. (2) is performed on all the possible masses, thus all the possible return periods are considered. Hence, a reference return period has not to be selected. On the contrary, the partial safety factor approach starts assuming a characteristic value of the mass, defined through its return period. With this purpose, three different reference return periods T_k, i.e. 50, 100 and 200 years, were considered and likewise series of simulations were performed adopting the sets of input parameters described in Sec. 3.1. Figure 2 graphically reports what observed in Table 1, displaying the boxplots for γ_H for the three T_k. As observed from what reported also in Table 1, the minimum and maximum values coincide with the whisker limits for all the T_k. A slightly left-skewed tendency is observed in all the cases, decreasing the interquartile range increasing T_k. Similarly, the spread of the distributions, i.e. the extent of the whiskers, decreases for greater T_k.

It emerges from the plot that the adoption of a T_k equal to 200 years decreases the range of variability of γ_H, as already observed for the energy [37], even more evidently. Considering $T_k = 200$ year as representative, and with the same p_f assumed in Sec. 3.1, parametric analyses were performed varying, in pairs, the values of h_{95}, h_{99}/h_{95}, the volume of the block M_{th}/ρ, λ, α, and N. Table 2 indicates the range of each variable. Each analysis was performed setting the not-varying parameters at the value reported in the third column of Table 2, which corresponds to the mean value of the correspondent range, except for $\lambda = 0.5$ and $N = 500$.
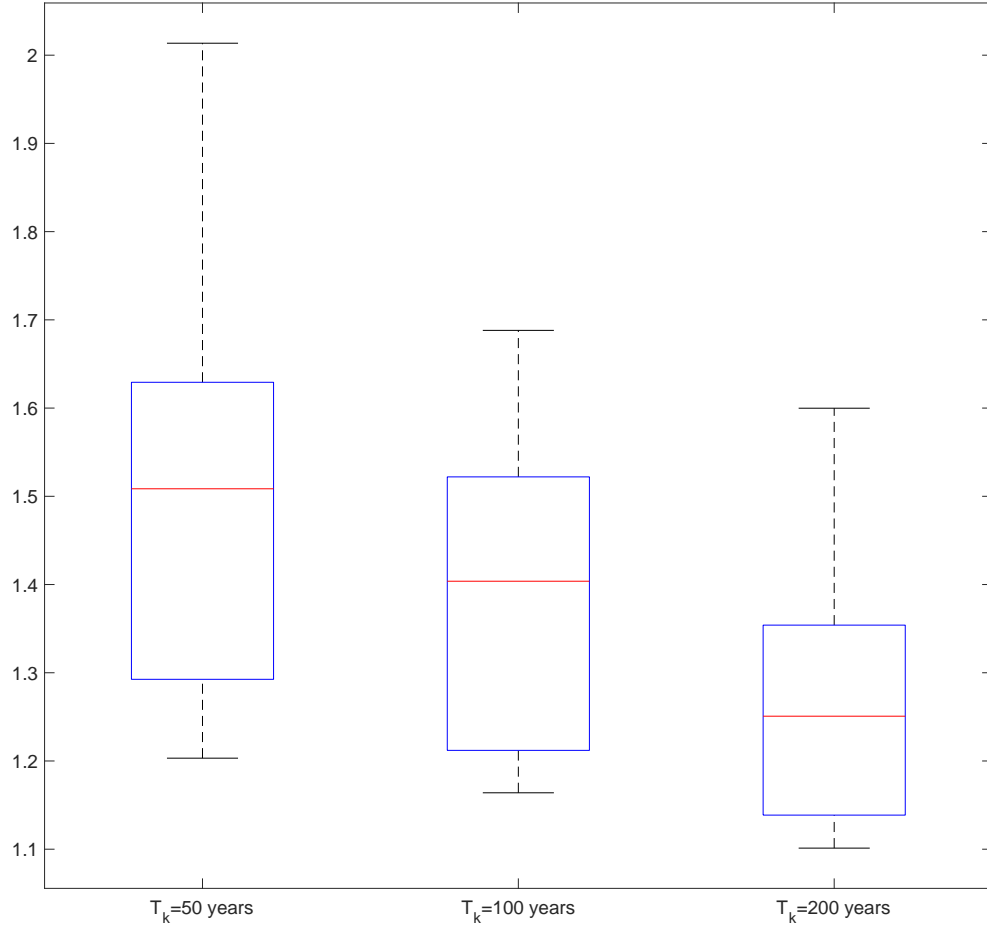
Figure 2: Boxplot of the partial safety factor γ_H for different reference return period $T_k = 50, 100, 200$ years.
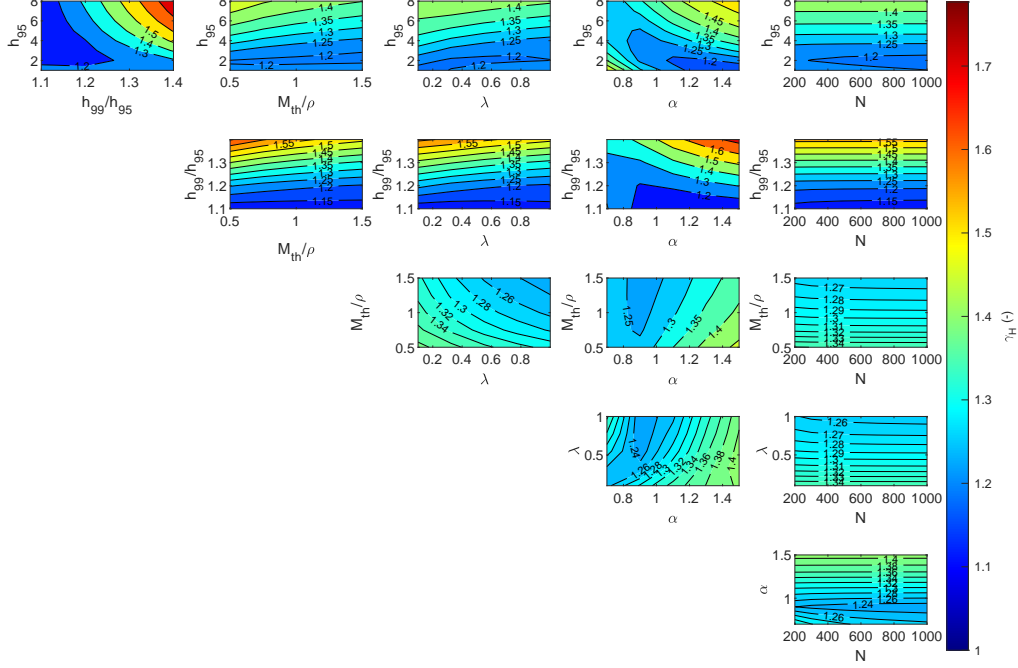
Figure 3: Contour plots of the partial safety factor γ_H, as function of h_{95}, h_{99}/h_{95}, V_{th}, λ, α, and N.

Figure 3 shows the contour plots of the partial safety factor γ_H for the 15 possible combinations of pair variables. To understand the plots, it has to be noted that the coefficient is independent from a variable represented on a given axis if the contour plot shows bounds parallel the corresponding axis. In this sense, it emerges that the dependence of γ_H on N is negligible for N greater than 200. As expected, the highest influence appears on h_{95} *vs* h_{99}/h_{95} plot. Increasing h_{99}/h_{95}, γ_H increases almost independently from M_{th}/ρ, λ and N. The pattern changes for the remaining variables, where larger increments are seen for high values of either h_{95} and α. The obtained values are within the bounds of the boxplot sketched in Figure 2, which reveals a maximum value of γ_H at about 1.6, and a median value at about 1.3.

Variable	Minimum	Maximum	Fixed value
h_{95} (m)	1	8	4.5
h_{99}/h_{95} (-)	1.1	1.4	1.25
M_{th}/ρ (m^3)	0.5	1.5	1
λ (event/year)	0.1	1	0.5
α (-)	0.7	1.5	1.1
N (-)	200	1000	500

Table 2: Range of the variables h_{95}, h_{99}/h_{95}, M_{th}/ρ, λ, α, and N adopted in the performed simulations.

5. Function fitting with a shallow neural network

In the previous section the influence of h_{95}, h_{99}/h_{95}, M_{th}/ρ, λ, α, N, and T_k on γ_H, given a p_f, was assessed. Similarly, in [36] the dependency of γ_E to v_{99}/v_{95}, α, N, and T_k was highlighted. The purpose of this section is to present a possible fitting for straightforwardly estimating γ_H and γ_E without performing the integrals reported in Sec. 2.

With this purpose 85000 simulations were performed applying the proposed time-dependent reliability method, with a Monte Carlo sampling technique of the input parameters, uniformly distributed in the range proposed in Table 3. This allowed to create a sample statistically significant of combinations of input and resulting outputs, in terms of both γ_H and γ_E. The creation of the dataset took 670 hours on a workstation with an Intel Silver Xeon 4214 2.2 GHz CPU.

Figures 4 and 5 plot an empirical density function of the obtained partial safety factors. The calculations for computing γ_E were performed according to the procedure briefly illustrated in Sec. 2.2 and fully detailed in De Biagi et al. [36]. Both the factors highlight a right-skewed distribution. Considering γ_H, for a first attempt, the obtained values can be fitted by a log-normal distribution, considering 0 as the starting point, i.e. fitting the expression $\gamma_H - 1$. On the contrary, the law that best fits γ_E appears to be the Type II Generalized Extreme Value distribution, i.e. with a shape parameter $k > 0$.

The results of the parametric analysis were used following the leading idea to build an input-output relationship that can be used to evaluate the partial safety factors, for a given p_f. The inputs of the 85000 performed simulations served for the supervised learning of a shallow neural network, adopting the obtained γ_H and γ_E as the sets target outputs. A two-layer feed-forward
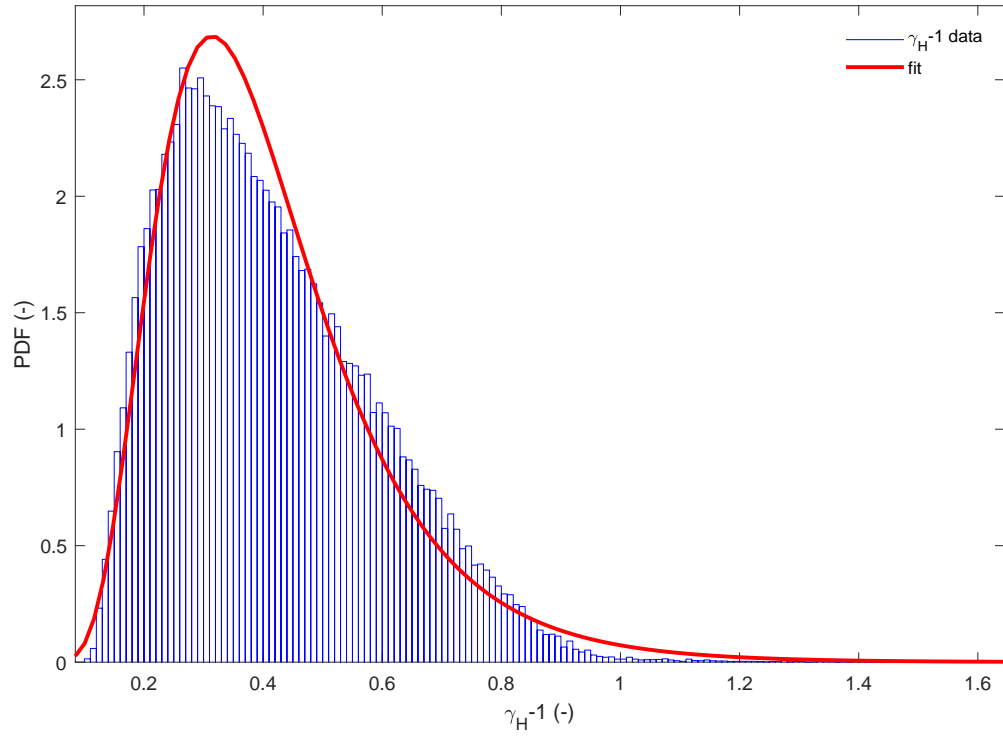
Figure 4: Obtained value of γ_H for the 85000 performed analyses with the time-dependent reliability approach. A lognormal fit of $(\gamma_H - 1)$ was proposed, with the mean of the logaritmic values $\mu = -0.972$ and the standard deviation of the logaritmic values $\sigma = 0.431$.
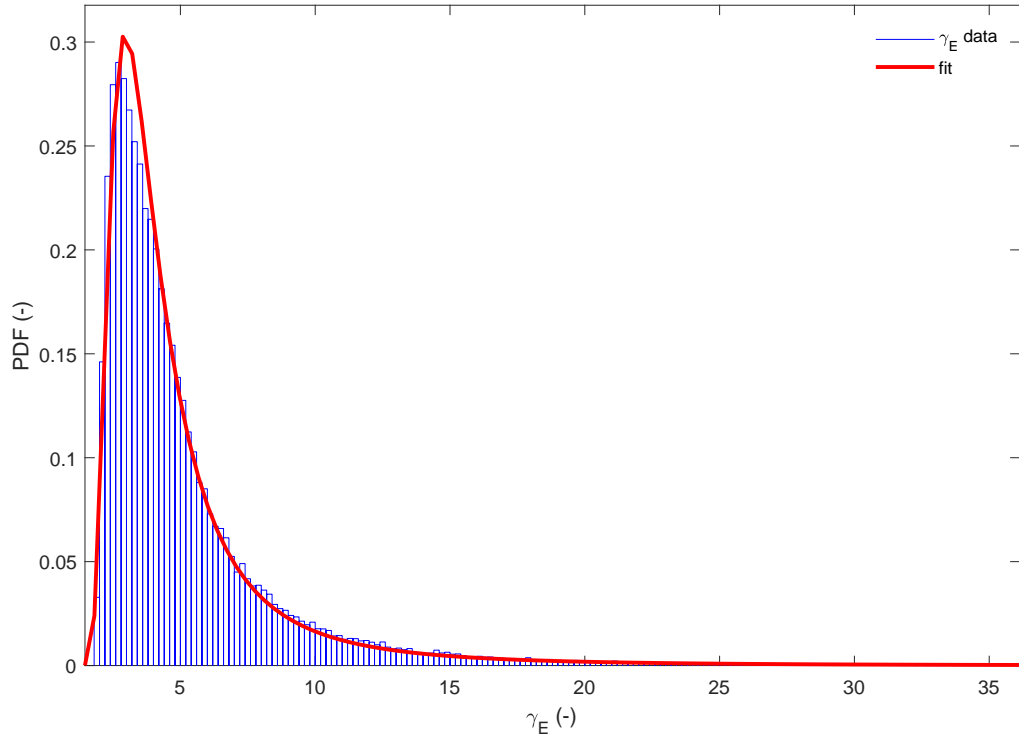
Figure 5: Obtained value of γ_E for the 85000 performed analyses with the time-dependent reliability approach. A generalized extreme value fit of γ_E was proposed, with the shape parameter $k = 0.477$, the scale parameter $\sigma = 1.335$, and the location parameter $\mu = 3.430$.

Variable	Values
h_{95} (m)	$1 - 8$
h_{99}/h_{95} (-)	$1.1 - 1.4$
v_{99}/v_{95} (-)	$1.01 - 1.4$
M_{th}/ρ (m^3)	$0.5 - 1.5$
λ (event/year)	$0.1 - 1$
α (-)	$0.7 - 1.5$
N (-)	$200 - 1000$
T_k (years)	$50 - 200$
v_9 (m/s)	20
ρ (kg/m^3)	2700

Table 3: Input parameters adopted in the performed simulations with a Monte Carlo sampling technique. The variables h_{95}, h_{99}/h_{95}, v_{99}/v_{95}, block volume M_{th}/ρ, λ, α, N, T_k span into the defied range, while v_{95} and ρ were kept fixed.

network with sigmoid hidden neurons and linear output neurons was built to fit these two multi-dimensional mapping problems, i.e. finding γ_H and γ_E, respectively. To briefly describe how the neural network works, for each hidden neuron, the inputs are weighted and summed, then a bias is associated. The resulting value is processed with a sigmoid transfer function, which output is combined with a linear transfer function with the outputs of all the hidden neurons, resulting in either γ_H or γ_E. A Matlab script was predisposed to model and train the neural network. In both cases, the networks were trained with Levenberg-Marquardt backpropagation algorithm, i.e. the Levenberg-Marquardt optimization was adopted to update weight and bias values of the network training function. The number of hidden neurons for each problem was chosen in order to maximize the goodness of the fit, i.e. an R-square greater than 0.99 was required. For this purpose 4 and 2 hidden neurons were used, respectively. The training of the network considered the 70% of the samples, a 15% of the samples were used to measure network generalization, and to halt training when generalization stops improving. In the end, the remaining 15% were used as test (for computing R-square statistics), providing an independent measure of network performance during and after training. Figure 6 displays the correlation between the network outputs (predicted γ values according to the created function fitting neural network) and the associated target values (the values computed with the time-dependent approach). The two regression plots show a lin-
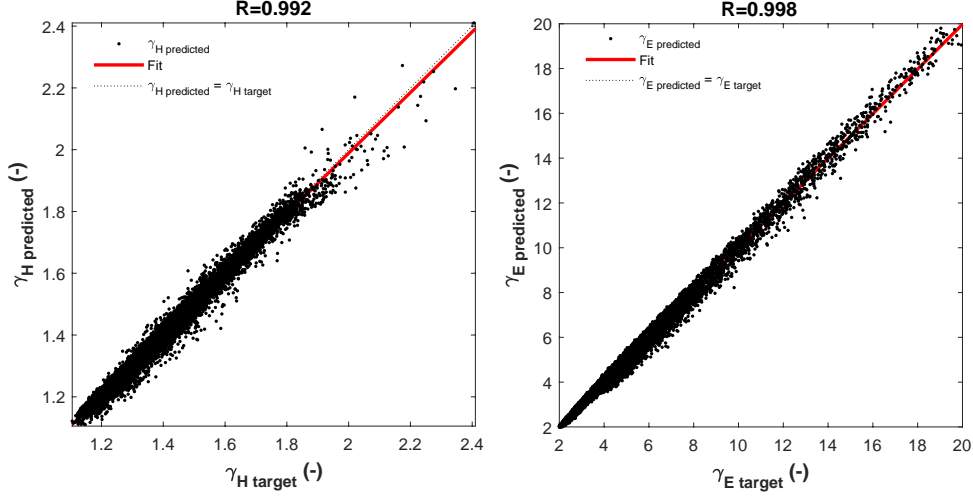
Figure 6: Goodness of the fitting function with the adopted shallow neural network to estimate γ_H and γ_E, for a given set of input parameters, for $p_f = 10^{-4}$.

ear fit to the adopted output-target relationships that closely intersect the bottom-left and top-right corners of the plot, i.e. when the outputs coincide with the target values (the slope is nearly one). The good fit is confirmed by the R-square values of 0.992 and 0.998 for γ_H and γ_E, respectively.

In Appendix A.1 and Appendix A.2, the Matlab neural network fitting functions are reported.

6. Conclusions

The time-dependent reliability approach introduced for the design of rock-fall passive measures [36] was enhanced accounting for the variability of the impacting block mass on the intercepting height of the system. Starting from the assumption that the failure of the system can occur for a kinetic energy or a trajectory height of the block greater than the interception capacity of the system, the proposed reliability-based approach takes into account the variability in time of the block mass and the uncertainties related to its kinematics and size.

Referring specifically to the height of the protection system, the approach was compared with the current semi-probabilistic ultimate limit state approach based on the application of partial safety factors. Three combinations of partial safety factors were proposed considering:

21

(i) different partial safety factors for each variable assuming a mutual independence between the two failure mode;

(ii) different partial safety factors for each variable adopting, for the mass, the same factor γ_{m_E} evaluated computing the failure related to the kinetic energy;

(iii) a unique safety factor for the effect of the actions, named γ_H.

Sensitivity analyses were performed, varying the most important input parameters, aiming at finding the most profitable and easy-to-use combination for the designer. The third combination reveals to be both straightforwards and to have the less dispersion, with maximum values around 2 for a reference return period of 50 years and an annual failure probability of 10^{-4}. Furthermore, the third combination allows to accounts for the effect of the resistance in a unique factor and, in the hypothesis to consider a δ-Dirac distribution of the resistance, it coincides with the partial safety factor associated with the effects of the actions only.

Once the partial safety factor unique for the effect of the actions, i.e. γ_H, was individuated as effective and easy-to-use, further sensitivity analyses were performed, with the purpose og deeply investigating the parameters which mostly affect its value. The h_{95}, h_{99}/h_{95} represent the variables which have the most influence, increasing which higher values of γ_H are obtained. On the contrary, for a significant number of surveyed blocks N, the influence of this last appears to be negligible. From the results it is suggested to adopt a reference return period for evaluating the characteristic mass equal to 200 years. In this framework, for p_f equal to 10^{-4} a value of γ_H equal to 1.6 can encompass the great variability of the input parameters, even though the site specificity of the impacting block mass and frequency of the event has always to be accurately evaluated.

With the purpose of preparing a tool that can be easily considered by the designer to get the partial safety factors, a shallow neural network was built and trained. The input values consist in the parameters of rockfall occurrence law and point values of the distribution of heights and velocities at the location of the protection system. The output are γ_H and γ_E, respectively, for a given p_f, i.e. 10^{-4}. The training dataset consisted in the results of a large number of simulations performed with the time-dependent reliability approach. The obtained fitting functions allow to estimate the partial safety factors with a very high goodness-of-fit, i.e. R-square greater than 0.99.

Further developments can focus on the definition of a correlation between kinetic energy and height accounting for propagation parameters, such as the

topography or the type of soil, or for the shape of the impacting block.

References

References

[1] C. Scavia, M. Barbero, M. Castelli, M. Marchelli, D. Peila, G. Torsello, G. Vallero, Evaluating rockfall risk: Some critical aspects, Geosciences (Switzerland) 10 (3) (2020) 1–29. `doi:10.3390/geosciences10030098`.

[2] P. Arnold, L. Dorren, The importance of rockfall and landslide risks on Swiss National Roads, Vol. 6, Spinger, 2015.

[3] R. Macciotta, C. D. Martin, D. M. Cruden, Probabilistic estimation of rockfall height and kinetic energy based on a three-dimensional trajectory model and monte carlo simulation, Landslides 12 (4) (2015) 757–772.

[4] O. Mavrouli, J. Corominas, Txt-tool 4.034-1.1: Quantitative rockfall risk assessment for roadways and railways, in: Landslide Dynamics: ISDR-ICL Landslide Interactive Teaching Tools, Springer, 2018, pp. 509–519.

[5] S. Mineo, Comparing rockfall hazard and risk assessment procedures along roads for different planning purposes, Journal of Mountain Science 17 (3) (2020) 653–669.

[6] A. Giacomini, K. Thoeni, E. Kniest, C. Lambert, In situ experiments of rockfall in an open pit coal mine, Proceeding of slope stability (2011) 1–11.

[7] K. Thoeni, A. Giacomini, S. Sloan, C. Lambert, D. Casagrande, Numerical analysis of rockfall hazard in open pit coal mines, in: Conference: Computer Methods for Geomechanics: Frontiers and New Application, University of Canterbury. Civil and Natural Resources Engineering, 2011, pp. 1151–1156.

[8] F. Ferrari, K. Thoeni, A. Giacomini, C. Lambert, A new rockfall hazard assessment methodology for open-pit coal mines, in: Bowen Basin Symposium, 2015, pp. 355–362.

[9] A. Giacomini, K. Thoeni, M. Santise, F. Diotri, S. Booth, S. Fityus, R. Roncella, Temporal-spatial frequency rockfall data from open-pit highwalls using a low-cost monitoring system, Remote Sensing 12 (15) (2020) 2459.

[10] F. Agliardi, G. B. Crosta, P. Frattini, Integrating rockfall risk assessment and countermeasure design by 3D modelling techniques, Natural Hazards and Earth System Science 9 (4) (2009) 1059–1073. `doi: 10.5194/nhess-9-1059-2009`.

[11] G. B. Crosta, F. Agliardi, P. Frattini, S. Lari, Key issues in rock fall modeling, hazard and risk assessment for rockfall protection, in: Engineering Geology for Society and Territory-Volume 2, Springer, 2015, pp. 43–58.

[12] D. Peila, C. Ronco, Design of rockfall net fences and the new etag 027 european guideline, Natural Hazards and Earth System Sciences 9 (4) (2009) 1291–1298.

[13] D. Bertrand, A. Trad, A. Limam, C. Silvani, Full-scale dynamic analysis of an innovative rockfall fence under impact using the discrete element method: From the local scale to the structure scale, Rock Mechanics and Rock Engineering 45 (5) (2012) 885–900.

[14] D. Toe, A. Mentani, L. Govoni, F. Bourrier, G. Gottardi, S. Lambert, Introducing meta-models for a more efficient hazard mitigation strategy with rockfall protection barriers, Rock mechanics and rock engineering 51 (4) (2018) 1097–1109.

[15] S. Lambert, B. Kister, B. Loup, Literature-based Expedient Criterion for Assessing the Impact Strength of Switzerland ' s Rockfall Protection Embankment Inventory, in: Symposium Proceedings of the Interpraevent 2018 in the Pacifi Rim, 2018, pp. 208–214.

[16] S. Lambert, B. Kister, Efficiency assessment of existing rockfall protection embankments based on an impact strength criterion, Engineering geology 243 (2018) 1–9.

[17] M. Marchelli, A quick-assessment procedure to evaluate the degree of conservation of rockfall net fences (in italian), GEAM. GEOINGEGNERIA AMBIENTALE E MINERARIA 160 (2020) 24–35.

[18] EAD 340059-00-0106, Falling rock protection kits (2018).

[19] D. Peila, C. Oggeri, C. Castiglia, Ground reinforced embankments for rockfall protection: Design and evaluation of full scale tests, Landslides 4 (3) (2007) 255–265. `doi:10.1007/s10346-007-0081-4`.

[20] S. Lambert, F. Bourrier, Design of rockfall protection embankments: A review, Engineering Geology 154 (2013) 77–88.

[21] X. Wang, P. Frattini, G. Crosta, L. Zhang, F. Agliardi, S. Lari, Z. Yang, Uncertainty assessment in quantitative rockfall risk assessment, Landslides 11 (4) (2014) 711–722.

[22] F. Bourrier, J. Baroth, S. Lambert, Accounting for the variability of rock detachment conditions in designing rockfall protection structures, Natural Hazards 81 (1) (2016) 365–385. `doi:10.1007/s11069-015-2084-0`.

[23] O. Mavrouli, J. Corominas, Comparing rockfall scar volumes and kinematically detachable rock masses, Engineering Geology 219 (2017) 64–73. `doi:10.1016/j.enggeo.2016.08.013`.

[24] F. Bourrier, S. Lambert, J. Baroth, A Reliability-Based Approach for the Design of Rockfall Protection Fences, Rock Mechanics and Rock Engineering 48 (1) (2014) 247–259. `doi:10.1007/s00603-013-0540-2`.

[25] L. Zhao, Z. X. Yu, Y. P. Liu, J. W. He, S. L. Chan, S. C. Zhao, Numerical simulation of responses of flexible rockfall barriers under impact loading at different positions, Journal of Constructional Steel Research 167 (2020) 105953. `doi:10.1016/j.jcsr.2020.105953`.
URL `https://doi.org/10.1016/j.jcsr.2020.105953`

[26] A. Mentani, A. Giacomini, O. Buzzi, L. Govoni, G. Gottardi, S. Fityus, Numerical modelling of a low-energy rockfall barrier: new insight into the bullet effect, Rock Mechanics and Rock Engineering 49 (4) (2016) 1247–1262.

[27] Z. Gao, H. Al-Budairi, A. Steel, Experimental testing of low-energy rockfall catch fence meshes, Journal of Rock Mechanics and Geotechnical Engineering 10 (4) (2018) 798–804.

[28] A. Volkwein, A. Roth, W. Gerber, A. Vogel, Flexible rockfall barriers subjected to extreme loads, Structural Engineering International: Journal of the International Association for Bridge and Structural Engineering (IABSE) 19 (3) (2009) 327–332. `doi:10.2749/101686609788957900`.

[29] R. C. Koo, J. S. Kwan, C. Lam, C. W. Ng, J. Yiu, C. E. Choi, A. K. Ng, K. K. Ho, W. Pun, Dynamic response of flexible rockfall barriers under different loading geometries, Landslides 14 (3) (2017) 905–916. `doi:10.1007/s10346-016-0772-9`.

[30] Z. X. Yu, L. Zhao, Y. P. Liu, S. C. Zhao, H. Xu, S. L. Chan, Studies on flexible rockfall barriers for failure modes, mechanisms and design strategies: a case study of Western China, Landslides 16 (2) (2019) 347–362. `doi:10.1007/s10346-018-1093-y`.

[31] P. Van Tran, K. Maegawa, S. Fukada, Experiments and dynamic finite element analysis of a wire-rope rockfall protective fence, Rock mechanics and rock engineering 46 (5) (2013) 1183–1198.

[32] X. Qi, Z. X. Yu, L. Zhao, H. Xu, S. C. Zhao, A new numerical modelling approach for flexible rockfall protection barriers based on failure modes, Advanced Steel Construction 14 (3) (2018) 479–495. `doi:10.18057/IJASC.2018.14.3.10`.

[33] J. B. Coulibaly, M.-A. Chanut, S. Lambert, F. Nicot, Toward a generic computational approach for flexible rockfall barrier modeling, Rock Mechanics and Rock Engineering 52 (11) (2019) 4475–4496.

[34] S. Lambert, F. Bourrier, D. Toe, Improving three-dimensional rockfall trajectory simulation codes for assessing the efficiency of protective embankments, International Journal of Rock Mechanics and Mining Sciences 60 (1365) (2013) 26–36. `doi:10.1016/j.ijrmms.2012.12.029`. URL `http://dx.doi.org/10.1016/j.ijrmms.2012.12.029`

[35] EN 1990:2002, Eurocode 0 - basis of structural design (2002).

[36] V. De Biagi, M. Marchelli, D. Peila, Reliability analysis and partial safety factors approach for rockfall protection structures, Engineering Structures 213 (September 2019) (2020) 110553. `doi:10.1016/j.`

engstruct.2020.110553.
URL https://doi.org/10.1016/j.engstruct.2020.110553

[37] M. Marchelli, V. De Biagi, D. Peila, Reliability-based design of protection net fences: Influence of rockfall uncertainties through a statistical analysis, Geosciences 10 (8) (2020) 280.

[38] EN 1997-1:2004, Eurocode 7 - geotechnical design. part 1: General rules (2004).

[39] V. De Biagi, M. L. Napoli, M. Barbero, A quantitative approach for the evaluation of rockfall risk on buildings, Natural hazards 88 (2017) 1059–1086.

[40] D. Piteau, R. Clayton, Computer rockfall model, in: Proceedings of the meeting on rockfall dynamics and protective works effectiveness, Bergamo, Italy, ISMES Publication, Vol. 90, 1976, pp. 123–125.

[41] D. Piteau, R. Clayton, Description of the slope model computer rock fall program for determining rock fall distribution, DR Piteau and Associates.

[42] S. Evans, O. Hungr, The assessment of rockfall hazard at the base of talus slopes, Canadian geotechnical journal 30 (4) (1993) 620–636.

[43] L. K. Dorren, A review of rockfall mechanics and modelling approaches, Progress in Physical Geography 27 (1) (2003) 69–87.

[44] V. De Biagi, M. L. Napoli, M. Barbero, D. Peila, Estimation of the return period of rockfall blocks according to their size, Natural Hazards and Earth System Sciences 17 (1) (2017) 103–113.

[45] D. Toe, A. Mentani, G. Gottardi, F. Bourrier, A Novel Approach to Assess the Ability of a Protection Barrier to Mitigate Rockfall Hazard, Symposium Proceedings of the INTERPRAENENT 2018 in the Pacific Rim (2018) 249–257.

[46] X. Qi, X. Pei, R. Han, Y. Yang, Q. Meng, Z. Yu, Analysis of the effects of a rotating rock on rockfall protection barriers, Geotechnical and Geological Engineering 36 (5) (2018) 3255–3267.

[47] R. E. Melchers, A. T. Beck, Structural reliability analysis and prediction, John Wiley & Sons, 2018.

[48] UNI 11211-4, Opere di difesa dalla caduta massi - parte 4: Progetto definitivo ed esecutivo (2018).

[49] ONR 24810, Technical protection against rockfall - terms and definitions, effects of actions, design, monitoring and maintenance (2017).

Appendix A. Shallow Neural Networks functions

In this Section the Matlab codes of the fitting functions of γ_H and γ_E are reported. The computed partial safety factor refer to a failure probability $p_f = 10^{-4}$. The output of the function corresponds to the value of the factor. The variables in the input vector are arranged as follows:

- x1(1): h_{95} in meters (m);

- x1(2): h_{99}/h_{95};

- x1(3): v_{99}/v_{95};

- x1(4): M_{th}/ρ in cubic meters (m^3);

- x1(5): λ in events per year (1/yr);

- x1(6): α;

- x1(7): N;

- x1(8): T_k in years (yrs);

Appendix A.1. Fitting function for the failure related to the intercepting height

```
1 function [y1] = NetworkFunction_gammaH(x1)
2 x1_step1.xoffset =
     [1.00007705139075;1.10000325627036;...
3     1.01000012450238;0.500022669004365;0.100022076771101;...

4     0.700000426754315;200.004539009949;50.0044576267548];
```

```matlab
5 x1_step1.gain = [0.285725210574242;6.66677449571979;...
6     100.001737957821;2.00006109248878;2.22233592364953;...

7     2.5000524617702;0.0025000793124972;0.0133340172249735];

8 x1_step1.ymin = −1;
9
10 b1 = [−0.96994424341848373139;2.4434931938144042185;...
11     0.93632230418068318478;2.6147332054610310514];
12 IW1_1 = [0.6626552369493338146  0.30114462942269037971
      0.0008056492358921626528  −0.10338475458880468094
      −0.23606786259033188391  0.723620148969206  78897
      0.02129765720507247 3979
      −0.081080858132982741582;0.4302835165370316739
      0.080747465725212963505  0.0022677400790091554149
      −0.061669127636850007423  −0.13984395884369371643
      0.62310571127428959759  0.04158525881886 4809238
      0.28680238300776356164;−0.6425289664266 0550786
      −0.32471469700949423531  −0.0007877082291 0222669262
      0.10217926565206587874  0.22524048868845417126
      −0.70136966545215106983  −0.0205776911390 44868018
      0.08039458294859647 1361;1.1553121021136427693
      −1.0949621524085095814  −0.0059651455104 693549766
      0.051857871447203142401  0.219771596426 96225683
      −1.1457661662696296823  −0.03639063861879 2062187
      −0.11853874833516518661];
13
14 b2 = 7.765402085535460408;
15 LW2_1 = [−12.773539096945890847  −8.5142788550969807915
      −13.408937654336398282  0.21433821914027162414];
16
17 y1_step1.ymin = −1;
18 y1_step1.gain = 1.31336136992816;
19 y1_step1.xoffset = 1.10423683202347;
20
21 Q = size(x1,1); % samples
22
23 x1 = x1';
```

29

```
24 xp1 = mapminmax_apply(x1, x1_step1);
25
26 a1 = tansig_apply(repmat(b1,1,Q) + IW1_1*xp1);
27
28 a2 = repmat(b2,1,Q) + LW2_1*a1;
29
30 % Output 1
31 y1 = mapminmax_reverse(a2, y1_step1);
32 y1 = y1';
33 end
34
35 % ===== MODULE FUNCTIONS ========
36 % Map Minimum and Maximum Input Processing Function
37 function y = mapminmax_apply(x, settings)
38 y = bsxfun(@minus, x, settings.xoffset);
39 y = bsxfun(@times, y, settings.gain);
40 y = bsxfun(@plus, y, settings.ymin);
41 end
42
43 % Sigmoid Symmetric Transfer Function
44 function a = tansig_apply(n,~)
45 a = 2 ./ (1 + exp(-2*n)) - 1;
46 end
47
48 % Map Minimum and Maximum Output Reverse-Processing
      Function
49 function x = mapminmax_reverse(y, settings)
50 x = bsxfun(@minus, y, settings.ymin);
51 x = bsxfun(@rdivide, x, settings.gain);
52 x = bsxfun(@plus, x, settings.xoffset);
53 end
```

Appendix A.2. Fitting function for the failure related to the energy absorption capacity

```
1 function [y1] = NetworkFunction_gammaE(x1)
2
3 x1_step1.xoffset =
      [1.00007705139075;1.10000325627036;...
```

```matlab
4        1.01000012450238;0.500022669004365;0.100022076771101;...

5        0.700000426754315;200.004539009949;50.0044576267548];

6 x1_step1.gain = [0.285725210574242;6.66677449571979;...
7        100.001737957821;2.00006109248878;2.22233592364953;...

8        2.5000524617702;0.0025000793124972;0.0133340172249735];

9 x1_step1.ymin = −1;
10
11 b1 = [−5.2355495278649977209;2.9935483207957438445];
12 IW1_1 = [4.3091351516700217931e−06
       0.00014938091770804072717  −0.018827107883444122588
       0.0013818303542731200789  0.044839727305480206465
       −1.4598652655344621643  −0.065346460756708399376
       −1.4479608354462660813;−4.9177503041436997023e−05
       0.00018293655394017440882  0.025189616948156488829
       3.1940124495348630083e−05  −0.04740379400783946325
       0.37330636595541399902  0.070505765509977738614
       0.41031632048195126883];
13
14 b2 = 83.32311606555633432;
15 LW2_1 = [53.245739252725059032  −31.104005154307117209];
16
17 y1_step1.ymin = −1;
18 y1_step1.gain = 0.0588983480590955;
19 y1_step1.xoffset = 1.80303653966967;
20
21 Q = size(x1,1); % samples
22
23 x1 = x1';
24 xp1 = mapminmax_apply(x1,x1_step1);
25
26 a1 = tansig_apply(repmat(b1,1,Q) + IW1_1*xp1);
27
28 a2 = repmat(b2,1,Q) + LW2_1*a1;
29
```

```
30 y1 = mapminmax_reverse(a2,y1_step1);
31 y1 = y1';
32 end
33
34 % Map Minimum and Maximum Input Processing Function
35 function y = mapminmax_apply(x,settings)
36 y = bsxfun(@minus,x,settings.xoffset);
37 y = bsxfun(@times,y,settings.gain);
38 y = bsxfun(@plus,y,settings.ymin);
39 end
40
41 % Sigmoid Symmetric Transfer Function
42 function a = tansig_apply(n,~)
43 a = 2 ./ (1 + exp(-2*n)) - 1;
44 end
45
46 % Map Minimum and Maximum Output Reverse-Processing
         Function
47 function x = mapminmax_reverse(y,settings)
48 x = bsxfun(@minus,y,settings.ymin);
49 x = bsxfun(@rdivide,x,settings.gain);
50 x = bsxfun(@plus,x,settings.xoffset);
51 end
```